



Pex30 undergoes phosphorylation and regulates peroxisome number in *Saccharomyces cerevisiae*

Nayan Moni Deori¹ · Terence Infant¹ · Pradeep Kumar Sundaravadivelu² · Rajkumar P. Thummer² · Shirisha Nagotu¹

Received: 18 November 2021 / Accepted: 8 February 2022 / Published online: 26 February 2022
© The Author(s), under exclusive licence to Springer-Verlag GmbH Germany, part of Springer Nature 2022

Abstract

Pex30 is a dysferlin domain-containing protein whose role in peroxisome biogenesis has been studied by several research groups. Notably, recent studies have linked this protein to peroxisomes, endoplasmic reticulum and lipid bodies in *Saccharomyces cerevisiae*. Phosphoproteome studies of *S. cerevisiae* have identified several phosphorylation sites in Pex30. In this study we expressed and purified Pex30 from its native host. Analysis of the purified protein by circular dichroism spectroscopy showed that it retained its secondary structure and revealed primarily a helical structure. Further phosphorylation of Pex30 at three residues, Threonine 60, Serine 61 and Serine 511 was identified by mass spectrometry in this study. To understand the importance of this post-translational modification in peroxisome biogenesis, the identified residues were mutated to both non-phosphorylatable (alanine) and phosphomimetic (aspartic acid) variants. Upon analysis of the mutant variants by fluorescence microscopy, no alteration in the localization of the protein to ER and peroxisomes was observed. Interestingly, reduced number of peroxisomes were observed in cells expressing phosphomimetic mutations when cultured in peroxisome-inducing conditions. Our data suggest that phosphorylation and dephosphorylation of Pex30 may promote distinct interactions essential in regulating peroxisome number in a cell.

Keywords Peroxisomes · Phosphorylation · ER · Pex30 · Mass spectrometry

Introduction

Protein phosphorylation is a ubiquitous post-translational modification that regulates various cellular processes in eukaryotes (Cohen 2002). Phosphorylation events are dynamic and reversible, mediated by protein kinases and phosphatases (Taylor et al. 2012). Protein phosphorylation involves introducing a negatively charged phosphate group to the side chain of a specific amino acid residue, mainly serine, threonine, and tyrosine, in a polypeptide chain (Hunter

2012). The addition of a covalently bound phosphate group results in conformational changes in the structure of the protein that leads to alteration in the binding affinity of the protein with its interacting partners and the regulation of subcellular localization of the protein (Johnson and Barford 1993; Nishi et al. 2011; Balta et al. 2018). Approximately 40–50% of yeast proteome is reported to be phosphorylated, indicating the indispensable nature of phosphorylation in the study of eukaryotic biology (Vlastaridis et al. 2017).

Peroxisomes are single membrane-bound organelles ubiquitously present in all eukaryotes whose number and function vary in response to cellular metabolic needs (Deb and Nagotu 2017). Peroxisomes are well-characterized for their role in neutralizing harmful reactive oxygen species (ROS) produced by the cell and the β -oxidation of fatty acids (Deb and Nagotu 2017; Deori et al. 2018). The biogenesis of these organelles is regulated by a set of proteins called peroxins (Pex) required for various aspects of biogenesis, such as division and protein import leading to the formation and maturation of new daughter peroxisomes (Subramani et al. 2000; Akşit and van der Klei 2018). Previous studies have

Communicated by Martine Collart.

✉ Shirisha Nagotu
snagotu@iitg.ac.in

¹ Organelle Biology and Cellular Ageing Lab, Department of Biosciences and Bioengineering, Indian Institute of Technology Guwahati, Guwahati-781039, Assam, India

² Laboratory for Stem Cell Engineering and Regenerative Medicine, Department of Biosciences and Bioengineering, Indian Institute of Technology Guwahati, Guwahati-781039, Assam, India

reported that Pex proteins are also associated with the degradation of peroxisomes termed pexophagy (Zutphen et al. 2008; Zhang et al. 2015). In *S. cerevisiae*, the differential identification of phosphorylated-proteins when cultured in peroxisome-inducing and peroxisome-repressing conditions emphasizes the relevance of phosphorylation on peroxisome dynamics (Saleem et al. 2010). Several peroxisomal proteins in various organisms are now reported to be phosphorylated (Infant et al. 2021). This modification regulates the import of peroxisomal proteins such as Cit2p (a peroxisomal isoform of citrate synthase) and catalase from the cytosol into the peroxisomal matrix (Oeljeklaus et al. 2016; Okumoto et al. 2020; Schummer et al. 2020). Phosphorylated forms of the peroxisomal membrane protein Pex11 are also identified in various yeast species (Knoblach and Rachubinski 2010; Joshi et al. 2012; Thomas et al. 2015).

One such interesting protein that is multifunctional and has a role in peroxisome biogenesis, lipid droplet biogenesis, and required for the maintenance of ER shape is Pex30 (Vizeacoumar et al. 2004; Joshi et al. 2016; Wang et al. 2018). Pex30 is a dysferlin domain-containing protein that initially targets to the cortical ER and then traffics to specific subdomains of ER where it associates with proteins responsible for maintaining the tubular structure of ER such as Rtn1, Rtn2 and Yop1 (David et al. 2013). Earlier studies have reported an increase in peroxisome number in cells lacking Pex30, thereby indicating its role in the regulation of peroxisome number in a cell (Vizeacoumar et al. 2004). However, later studies reported the role of Pex30 in the formation of peroxisomes from the ER (David et al. 2013). A role for Pex30 in lipid body biogenesis has also been recently demonstrated. Pex30 is reported to associate with the lipid droplet protein, seipin, in specific subdomains of ER and modulates the exit site of pre-peroxisomal vesicles (PPVs) that eventually leads to the formation of peroxisomes and lipid droplets (LDs) (Joshi et al. 2018). The absence of Pex30 is also associated with a delay in the formation of LDs

from the ER, underlying the role of Pex30 in LD biogenesis (Wang et al. 2018).

Several independent phosphoproteome studies have identified 17 putative residues in Pex30 that can undergo phosphorylation. Most of these phosphorylated sites are located at the extreme C-terminus of the protein (Albuquerque et al. 2008; Swaney et al. 2013; Lanz et al. 2021). Although Pex30 is reported to be phosphorylated at multiple residues, detailed studies of these putative sites on the function and localization of the protein are not performed. In this study, we identified the residues that undergo phosphorylation in Pex30. Further, we demonstrated that this post-translational modification of the protein is not needed for its expression and localization to peroxisomes and ER. Interestingly, the phosphomimetic variants of the protein exhibit significant reduction in the number of peroxisomes. Our data highlight the role of Pex30 in the regulation of peroxisome number.

Materials and methods

Yeast strains and plasmids

The plasmids and primers used in this study are listed in Tables 1, 2. The Pex30 gene was amplified using the primer pair pr-NMD001 and pr-NMD002 and *S. cerevisiae* BY4742 genomic DNA as a template. The amplified product was then fused to GFP at the C-terminus and expressed under the *MET25* promoter of the pUG35 vector. The resulting construct was verified by sequencing and then transformed into BY4742 pex30 Δ by lithium acetate (LiAc) method (Gietz and Sugino 1988). All strains used are isogenic to BY4742 (MAT α *his3 Δ 1 leu2 Δ 0 lys2 Δ 0 ura3 Δ 0*) and are listed in Table 3. pex30 Δ was obtained from the gene deletion library (Dharmacon). For colocalization experiments, plasmid pSM1959 and pUG34DsRed.SKL was used to mark ER and

Table 1 Plasmids used in this study

Plasmid	Description	Source
pUG35GFP	$P_{MET25}GFP$; amp ^R ; <i>Sc-URA3</i>	From Prof. Johannes Hegemann
pUG35-Pex30-GFP (pNMD001)	$P_{MET25}Pex30 GFP$; amp ^R ; <i>Sc-URA3</i>	This study
pUG34-DsRed.SKL	$P_{MET25}DsRed.SKL$; amp ^R ; <i>Sc-HIS3</i>	(Kuravi et al. 2006)
pSM1959	Sec63 mRFP; amp ^R ; <i>Sc-LEU2</i>	Addgene plasmid 41837 (Metzger et al. 2008)
pUG35-Pex30 ^{T60AS61A} GFP (pNMD0012)	$P_{MET25}Pex30^{T60AS61A} GFP$; amp ^R ; <i>Sc-URA3</i>	This study
pUG35-Pex30 ^{S511A} GFP (pNMD013)	$P_{MET25}Pex30^{S511A} GFP$; amp ^R ; <i>Sc-URA3</i>	This study
pUG35-Pex30 ^{T60AS61AS511A} GFP (pNMD0014)	$P_{MET25}Pex30^{T60AS61AS511A} GFP$; amp ^R ; <i>Sc-URA3</i>	This study
pUG35-Pex30 ^{T60DS61D} GFP (pNMD0015)	$P_{MET25}Pex30^{T60DS61D} GFP$; amp ^R ; <i>Sc-URA3</i>	This study
pUG35-Pex30 ^{S511D} GFP (pNMD016)	$P_{MET25}Pex30^{S511D} GFP$; amp ^R ; <i>Sc-URA3</i>	This study
pUG35-Pex30 ^{T60DS61DS511D} GFP (pNMD0017)	$P_{MET25}Pex30^{T60DS61DS511D} GFP$; amp ^R ; <i>Sc-URA3</i>	This study

Table 2 Primers used in this study

Primer	Sequence
pr-NMD001	5'-TGCTCTAGAATGAGTGGTAACACAACACTAACG-3'
pr-NMD002	5'-TCCCCCGGGTACGGCCTTCTTGCTATCG-3'
pr-NMD023	5'-GAAAGTTAACGTAGCTGCAGCGCCGCTTTTGACATC-3'
pr-NMD024	5'-GATGTCAAAGCGGGCTGCAGCTACGTTAACTTTC-3'
pr-NMD025	5'-GAAGAGAAAAGCAAGCAAATCCAACAATTGGTCGCGATAGC-3'
pr-NMD026	5'-GCTATCGCGACCAATTGTTGGATTGCTTGCTCTTCTCTTC-3'
pr-NMD027	5'-GGTCATTGGAGAAAGTTAATGTAGCTGATGATCCGCTTTTGACATCA-3'
pr-NMD028	5'-TGATGTCAAAGCGGATCATCAGCTACATTAACCTTCTCCAATGACC-3'
pr-NMD029	5'-GAAGAGAAAAGCAAGATAATCCAACAATTGGTCGCGATAGC-3'
pr-NMD030	5'-GCTATCGCGACCAATTGTTGGATTATCTTGCTCTTCTCTTC-3'

Table 3 *S. cerevisiae* strains used in this study

Strain	Description	Source
BY4742 WT	MAT α <i>his3</i> Δ <i>leu2</i> Δ <i>lys</i> Δ <i>ura3</i> Δ	Dharmacon
BY4742 <i>pex30</i> Δ	MAT α <i>his3</i> Δ <i>leu2</i> Δ <i>lys</i> Δ <i>ura3</i> Δ <i>pex30</i> Δ	Dharmacon
Y258::Pex30-His-HA	MAT α <i>pep4-3 his4-580 leu2-3112. URA3::Pex30-His-HA</i>	Dharmacon
BY4742 <i>pex30</i> Δ Pex30-GFP	BY4742 <i>pex30</i> Δ . URA3::P _{MET25} Pex30-GFP	This study
BY4742 <i>pex30</i> Δ Pex30-GFP DsRed.SKL	BY4742 <i>pex30</i> Δ . URA3::P _{MET25} Pex30-GFP.HIS: DsRed.SKL	This study
BY4742 <i>pex30</i> Δ Pex30-GFP Sec63-mRFP	BY4742 <i>pex30</i> Δ . URA3::P _{MET25} Pex30-GFP.LEU: Sec63-mRFP	This study
BY4742 <i>pex30</i> Δ Pex30 ^{T60AS61A} -GFP	BY4742 <i>pex30</i> Δ . URA3::P _{MET25} Pex30 ^{T60AS61A} GFP	This study
BY4742 <i>pex30</i> Δ Pex30 ^{S511A} -GFP	BY4742 <i>pex30</i> Δ . URA3::P _{MET25} Pex30 ^{S511A} GFP	This study
BY4742 <i>pex30</i> Δ Pex30 ^{T60AS61AS511A} -GFP	BY4742 <i>pex30</i> Δ . URA3::P _{MET25} Pex30 ^{T60AS61AS511A} GFP	This study
BY4742 <i>pex30</i> Δ Pex30 ^{T60AS61A} -GFP DsRed.SKL	BY4742 <i>pex30</i> Δ . URA3::P _{MET25} Pex30 ^{T60AS61A} GFP.HIS: DsRed.SKL	This study
BY4742 <i>pex30</i> Δ Pex30 ^{S511A} -GFP DsRed.SKL	BY4742 <i>pex30</i> Δ . URA3::P _{MET25} Pex30 ^{S511A} GFP.HIS: DsRed.SKL	This study
BY4742 <i>pex30</i> Δ Pex30 ^{T60AS61AS511A} -GFP DsRed.SKL	BY4742 <i>pex30</i> Δ . URA3::P _{MET25} Pex30 ^{T60AS61AS511A} GFP.HIS: DsRed.SKL	This study
BY4742 <i>pex30</i> Δ Pex30 ^{T60AS61A} -GFP Sec63-mRFP	BY4742 <i>pex30</i> Δ . URA3::P _{MET25} Pex30 ^{T60AS61A} GFP.LEU: Sec63-mRFP	This study
BY4742 <i>pex30</i> Δ Pex30 ^{S511A} -GFP Sec63-mRFP	BY4742 <i>pex30</i> Δ . URA3::P _{MET25} Pex30 ^{S511A} GFP.LEU: Sec63-mRFP	This study
BY4742 <i>pex30</i> Δ Pex30 ^{T60AS61AS511A} -GFP Sec63-mRFP	BY4742 <i>pex30</i> Δ . URA3::P _{MET25} Pex30 ^{T60AS61AS511A} GFP.LEU: Sec63-mRFP	This study
BY4742 <i>pex30</i> Δ Pex30 ^{T60DS61D} -GFP	BY4742 <i>pex30</i> Δ . URA3::P _{MET25} Pex30 ^{T60DS61D} GFP	This study
BY4742 <i>pex30</i> Δ Pex30 ^{S511D} -GFP	BY4742 <i>pex30</i> Δ . URA3::P _{MET25} Pex30 ^{S511D} GFP	This study
BY4742 <i>pex30</i> Δ Pex30 ^{T60DS61DS511D} -GFP	BY4742 <i>pex30</i> Δ . URA3::P _{MET25} Pex30 ^{T60DS61DS511D} GFP	This study
BY4742 <i>pex30</i> Δ Pex30 ^{T60DS61D} -GFP DsRed.SKL	BY4742 <i>pex30</i> Δ . URA3::P _{MET25} Pex30 ^{T60DS61D} GFP.HIS: DsRed.SKL	This study
BY4742 <i>pex30</i> Δ Pex30 ^{S511D} -GFP DsRed.SKL	BY4742 <i>pex30</i> Δ . URA3::P _{MET25} Pex30 ^{S511D} GFP.HIS: DsRed.SKL	This study
BY4742 <i>pex30</i> Δ Pex30 ^{T60DS61DS511D} -GFP DsRed.SKL	BY4742 <i>pex30</i> Δ . URA3::P _{MET25} Pex30 ^{T60DS61DS511D} GFP.HIS: DsRed.SKL	This study
BY4742 <i>pex30</i> Δ Pex30 ^{T60DS61D} -GFP Sec63-mRFP	BY4742 <i>pex30</i> Δ . URA3::P _{MET25} Pex30 ^{T60DS61D} GFP.LEU: Sec63-mRFP	This study
BY4742 <i>pex30</i> Δ Pex30 ^{S511D} -GFP Sec63-mRFP	BY4742 <i>pex30</i> Δ . URA3::P _{MET25} Pex30 ^{S511D} GFP.LEU: Sec63-mRFP	This study
BY4742 <i>pex30</i> Δ Pex30 ^{T60DS61DS511D} -GFP Sec63-mRFP	BY4742 <i>pex30</i> Δ . URA3::P _{MET25} Pex30 ^{T60DS61DS511D} GFP.LEU: Sec63-mRFP	This study

peroxisomes, respectively. Plasmid pSM1959 enables the expression of Sec63-mRFP (Addgene plasmid ID: 41837, (Metzger et al. 2008)) and plasmid pUG34DsRed.SKL enables MET25-driven expression of DsRed.SKL (Kuravi et al. 2006).

Growth conditions

S. cerevisiae cells were grown in (1) complete media containing 1% yeast extract, 2% bacteriological peptone and 1% glucose, (2) selective media (YND) containing 0.17% yeast

nitrogen base without amino acids, 0.5% ammonium sulfate, 2% glucose and pH adjusted to 6.0. Whenever necessary, media was supplemented with leucine (3 mg/ml), lysine (10 mg/ml) and histidine (10 mg/ml) (Kuravi et al. 2006). For growth on plates, 2% agar was added to the media. In brief, cells were grown at 30 °C and 200 rpm overnight and shifted to fresh medium and subsequently grown at 30 °C till they reached exponential growth phase. Cells were further shifted to fresh medium two times. All microscopic experiments were performed by analyzing exponentially growing cells. To induce peroxisomes, cells were grown in oleic acid-containing media (OA) media consisting of 0.17% yeast nitrogen base without amino acids, 0.5% ammonium sulfate, 0.1% glucose, 0.1% yeast extract, 0.1% oleic acid, 0.05% Tween-80 and pH adjusted to 6.0. Cells were cultured for a minimum of 8 h and subsequently analyzed.

Purification of His-tagged Pex30

S. cerevisiae cells expressing Pex30 tagged to hexa-histidine at its C-terminus under the control of an inducible galactose promoter were cultured in YND liquid medium supplemented with isoleucine (30 mg/L), valine (150 mg/L), arginine (20 mg/L), adenine (20 mg/L), histidine (20 mg/L), leucine (30 mg/L), lysine (30 mg/L), methionine (20 mg/L), phenylalanine (50 mg/L), tryptophan (20 mg/L) and tyrosine (30 mg/L). Cells were grown at 30 °C and 200 rpm overnight and were subsequently shifted to a fresh medium containing 2% raffinose. These cells were cultured till 1.2 OD₆₀₀ units in raffinose media after which 3 × yeast extract-peptone (YP) with 6% galactose was added to the media (final culture volume of 750 ml) and incubated for 6 h in growth conditions as per instructions provided in Yeast ORF collection manual (<https://horizondiscovery.com/-/media/Files/Horizon/resources/Technical-manuals/yeast-orf-collection-manual.pdf>). The induced cells were then harvested by centrifugation at 10,000 rpm for 10 min and subsequently, the pellet was resuspended in lysis buffer with protease and phosphatase inhibitors (50 mM Tris–HCl (pH 7.5), 300 mM NaCl, 0.1% Triton X-100, 0.1% β-mercaptoethanol, 1 mM PMSF, 1 × protease inhibitor cocktail without EDTA [Sigma-Aldrich] and 1 × phosphatase inhibitor cocktail [Sigma-Aldrich]) (Smaczynska-de Rooij Iwona et al. 2016). The resuspended cells were transferred to a screw-capped microcentrifuge tube to which zirconia beads corresponding to 1/3rd volume of the cell suspension were added. The cells were disrupted by vortexing for 15–20 cycles of 30 s beating and 1 min rest (for cooling). The cell lysate was subjected to mild centrifugation at 2000 rpm, 4 °C for 5 min. The supernatant was collected and mixed with Ni–NTA-charged resin pre-calibrated with equilibration buffer containing 30 mM imidazole. The matrix-bound His-conjugated Pex30 protein was eluted with two different concentrations

of imidazole viz. 300 and 500 mM. Stringent washing of the column with 40, 60 and 80 mM imidazole concentrations was performed prior to elution. The eluted samples were run on a conventional 10% sodium dodecyl sulfate–polyacrylamide gel electrophoresis (SDS-PAGE) gel and stained with Coomassie brilliant blue G-250 and the purified Pex30 band was excised for mass spectrometry (MS) analysis. The MS analysis was performed by the Proteomics Facility, Institute of Bioinformatics (IOB), Bangalore, India.

Circular dichroism spectroscopy

The eluted protein samples were pooled and desalted in 20 mM phosphate buffer using PD10 columns (GE healthcare) according to manufacturer's instructions prior to circular dichroism (CD) spectroscopy. Far-ultraviolet (UV) CD spectroscopy was performed to analyze the secondary structure of Pex30 as described previously (Haridhasapavan et al. 2021). Briefly, J-1500 spectropolarimeter (Jasco, Japan) equipped with a thermoelectric cooling-based temperature control unit was used under continuous nitrogen purging. The far-UV CD spectrum was recorded from 260 to 190 nm wavelength at a scan rate of 100 nm/min with a data integration time of 1 s. The spectrum was determined as an average of ten accumulations in a quartz cuvette of pathlength 0.1 cm. The phosphate buffer in which the protein was desalted, was used as a blank for background subtraction and the resulting spectrum was analyzed using BeStSel online tool (Micsnai et al. 2015, 2018).

Mass spectrometry (MS)

In-gel digestion

The excised gel fragment was subjected to a destaining solution of 40 mM ammonium bicarbonate (Sigma-Aldrich) and 40% (v/v) acetonitrile (Merck Millipore). Once the gel fragments were completely destained, 0.5 ml of 100% acetonitrile was added and incubated for 10–15 min until the gel slice shrunk and became opaque. After destaining, a reduction solution of 5 mM dithiothreitol (Sigma-Aldrich) in ammonium bicarbonate was added to the gel fragment and incubated at 60 °C for 30 min. This was followed by incubation of the gel fragment in an alkylation solution consisting of 20 mM iodoacetamide (Sigma-Aldrich) in 40 mM ammonium bicarbonate for 10 min at room temperature in the dark. The gel fragment was then dehydrated in 100% acetonitrile solution followed by digestion with trypsin (Promega) overnight at 37 °C. Following overnight digestion, the peptides were extracted using an extraction buffer consisting of 5% formic acid (Merck Millipore) and 40% acetonitrile. The

final peptide extraction was performed in 100% acetonitrile solution, followed by subjecting the pooled extract to vacuum-dry in a SpeedVac.

LC–MS/MS analysis

Reconstitution of the dried peptides was performed in 0.1% formic acid. The reconstituted peptides were then analyzed using Orbitrap Fusion Tribrid™ (Thermo Scientific™, Bremen, Germany) mass spectrometer coupled with Proxeon Easy nLC system (Thermo Scientific™, Bremen, Germany). Peptide enrichment was achieved by allowing the protein fragments to pass through at a flow rate of 3 μ L/min on to an Acclaim™ PepMap™ trap column (2 cm \times 75 μ m, Magic C₁₈AQ, 5 μ m, 100 Å, Michrom Biosciences Inc.). Peptides were separated on an analytical column (10 cm \times 75 μ m, Magic C₁₈AQ, 3 μ m, 100 Å, Mi-chrom Biosciences Inc.) at a flow rate of 350 nL/min employing a linear gradient of 5–32% acetonitrile for 40 min with a total run time of 60 min. MS and MS/MS scan acquisitions were executed in the Orbitrap mass analyzer at a mass resolution of 120,000 and 15,000 at 200 m/z, respectively. MS spectra were acquired in a data-dependent manner targeting the twenty most abundant ions with charge state ≥ 2 in each survey scan in the m/z range of 350–1600. Fragmentation was carried out using higher-energy collisional dissociation mode with normalized collision energy of 34. Isolation width was set to 1.6 m/z with 0.5 m/z offset. Precursor ions selected for MS/MS fragmentation were dynamically excluded for 30 s. The automatic gain control for full MS and MS/MS was set to 4×10^5 and 1×10^5 ions, respectively. The maximum ion injection time for full MS and MS/MS was set to 50 ms and 75 ms, respectively. Internal calibration was carried out by enabling lock mass option using polydimethylcyclsiloxane (m/z, 445.120025) ions (Olsen et al. 2005).

Data analysis

The mass spectrometry data were searched against *Saccharomyces* genome database and analyzed using Mascot (version 2.2.0, Matrix Science, London, UK) and SequestHT algorithm and Proteome Discoverer software (Version 1.4.0.288, Thermo Fisher Scientific). The analyzing criteria were set as oxidation of methionine and phosphorylation modification of serine, threonine and tyrosine as variable modifications and carbamidomethyl modification of cysteine as fixed modification. A 10 ppm of precursor mass tolerance, 0.02 Da of fragment mass tolerance and a maximum of two

missed cleavages were allowed. The spectral match hits were screened with 1% false discovery rate at the peptide level.

Phosphatase treatment and Phos-tag SDS-PAGE

The purified Pex30 was treated with three units of calf intestinal alkaline phosphatase (CIAP) (Promega) and incubated at 37 °C for 30 min. Elution fractions of Pex30 without CIAP were taken as control. Proteins from the above enzymatic reactions were separated using a 10% SDS-PAGE with the addition of 50 μ M Phos-tag (Wako Chemicals) and 100 μ M MnCl₂ in the resolving gel (Kinoshita et al. 2009). Electrophoretic separation was carried out at 80 V for 4 h. After electrophoresis, the gel was soaked with gentle agitation first in transfer buffer (25 mM Tris, 192 mM glycine, 10% methanol, pH 8.3) with 1 mM EDTA for 10 min, and subsequently with transfer buffer without EDTA. Proteins were transferred onto a nitrocellulose membrane at 20 V for 30 min.

Western blotting

For protein expression studies, cells corresponding to 3 OD₆₀₀ units of each strain were lysed by trichloroacetic acid method and this crude yeast extract was used for SDS-PAGE (Baerends et al. 2000). Briefly, cell pellet from culture corresponding to 3 OD₆₀₀ units was resuspended in 50% TCA and incubated for 30 min at – 80 °C. The cells were then washed twice with ice-cold 80% acetone. After air-drying the pellet at room temperature, the pellet was finally dissolved in 1% SDS/0.1 N sodium hydroxide solution. Lowry's method of protein estimation was used to estimate the amount of protein and an equal amount of protein was loaded onto each well (Lowry et al. 1951). The gels were run at a constant voltage of 130 V and transferred onto nitrocellulose membrane using Bio-Rad Trans-Blot®Turbo™. The membrane was first incubated with a blocking solution (5% skimmed milk) at room temperature for 2 h. The blots were probed with rabbit anti-GFP polyclonal antibody (1:5000) (Biobharti Life Science, Kolkata, India) and incubated overnight at 4 °C. For detection of His-tagged protein, blots were probed with an anti-his polyclonal antibody (1:5000) (Biobharti Life Science, Kolkata, India). Detection of GAPDH and β -actin were done by probing the blot with anti-GAPDH (1:5000) (Biobharti Life Science, Kolkata, India) and anti- β -actin polyclonal antibody (1:5000) (Invitrogen, Thermo Fisher Scientific, US). Goat anti-rabbit IgG (1:5000) or anti-mouse IgG (1:5000) conjugated to horseradish peroxidase (Invitrogen, Thermo Fisher Scientific, US) was used as secondary antibody for detection. Blots were developed

using Bio-Rad ECL substrate and captured using the Bio-Rad ChemiDoc™ XRS + system.

Site-directed mutagenesis

To generate non-phosphorylatable variants of Pex30, targeted mutations were introduced by following a two-stage PCR method using the *Pfu* Turbo DNA polymerase (Agilent Technologies, USA) as described by Wang and Malcolm (Wang and Malcolm 1999). Briefly, the stage-1 PCR involves two separate extension reactions performed in two separate tubes, one containing the forward primer and the other containing the reverse primer. A 20 ng template plasmid DNA was amplified by the following thermal cycler conditions: 2 min, 95 °C initial denaturation; 30 s, 95 °C denaturation step; 30 s, 60 °C, 62 °C and 65 °C annealing step followed by 16 min extension step. The two independent reactions were performed for 10 cycles. Subsequently, the two reactions were mixed and further amplification was performed for another 20 cycles. Finally, the terminal extension was performed for 10 min, 72 °C. Primers and template DNA used for generation of the plasmids carrying desired mutations is given in Table 4. The resulting plasmids containing phosphomimetic and non-phosphorylatable variants of Pex30 were confirmed by restriction digestion using specific restriction enzymes followed by DNA sequencing analysis. All the obtained plasmids were then separately transformed into *pex30Δ S. cerevisiae* cells by lithium-acetate transformation method and the recombinant clones were selected (Gietz and Sugino 1988).

Fluorescence microscopy

Fluorescence microscopy experiments were performed using an Olympus IX83 inverted microscope equipped with DP80 camera. A Plan-APOCHROMAT 100x/1.4 objective

Table 4 Primers and template DNA used for site-directed mutagenesis

Plasmid	Mutation	Primer pair	Template
pNMD012	T60AS61A	pr-NMD023 pr-NMD024	pNMD001
pNMD013	S511A	pr-NMD025 pr-NMD026	pNMD001
pNMD014	T60AS61AS511A	pr-NMD025 pr-NMD026	pNMD012
pNMD015	T60DS61D	pr-NMD027 pr-NMD028	pNMD001
pNMD016	S511D	pr-NMD029 pr-NMD030	pNMD001
pNMD017	T60DS61DS511D	pr-NMD029 pr-NMD030	pNMD015

was used for image acquisition. Samples were illuminated using pE-300^{white}CoolLED light source and GFP was visualized using U-FBNA filter with excitation range: 470–495 nm, dichroic: 505 nm and emission: 510–550 nm. RFP was visualized using a brightline triple-bandpass filter 378/474/575 nm (Semrock) with dichroic beamsplitter 409/493/596 nm (Semrock). All images were captured at room temperature and processed using Cellsens software (version 2.3). For co-localization experiments, cells were fixed with 4% formaldehyde in phosphate-buffered saline, pH 7.4 (PBS) for 30 min on ice. The *z* axis stacks were obtained starting from top to bottom of yeast cells with the stacks spaced 0.3 μm apart. The final images were assembled in Adobe Photoshop 7.0. Individual cells in the images were marked by using the “multi-point” tool of ImageJ for quantification. Quantification of the number of peroxisomes was done by counting peroxisomes in 40 random non-budding yeast cells from each experiment. Two independent experiments were considered for the analysis.

Statistical analysis

Quantitative analysis was performed from at least two independent biological experiments. Student's *t* test or two-way analysis of variance (ANOVA) was used for multiple comparisons. Error bar indicates the mean ± SEM. Values of $P < 0.05$ were considered significant (*), $P < 0.01$ very significant (**), and $P < 0.001$ extremely significant (***). The data were analyzed using GraphPad prism 8.2.4.

Results

Expression of Pex30 differs in media containing glucose and oleic acid as carbon source

Peroxisomes are involved in the β-oxidation of fatty acids, and therefore, the function of these organelles can be studied in media containing OA as a carbon source (Kunau et al. 1995; Poirier et al. 2006; Deb and Nagotu 2017). As it was reported in previous studies that the association between Pex30 and peroxisomes differs in glucose and OA media (Mast et al. 2016), we sought to analyze the expression of Pex30 in both peroxisome non-inducing (YND) and inducing growth conditions (OA). The Pex30-GFP construct was transformed into *pex30Δ* cells and subsequently expression was examined by fluorescence microscopy and western blotting. Interestingly, microscopic analysis revealed a difference in the phenotype of Pex30-GFP in cells grown in YND and OA media. Reticulate distribution of GFP around the cell periphery along with discrete GFP puncta was observed in almost all the cells cultured in YND media. On the other hand, cells grown in OA medium exhibited two distinct

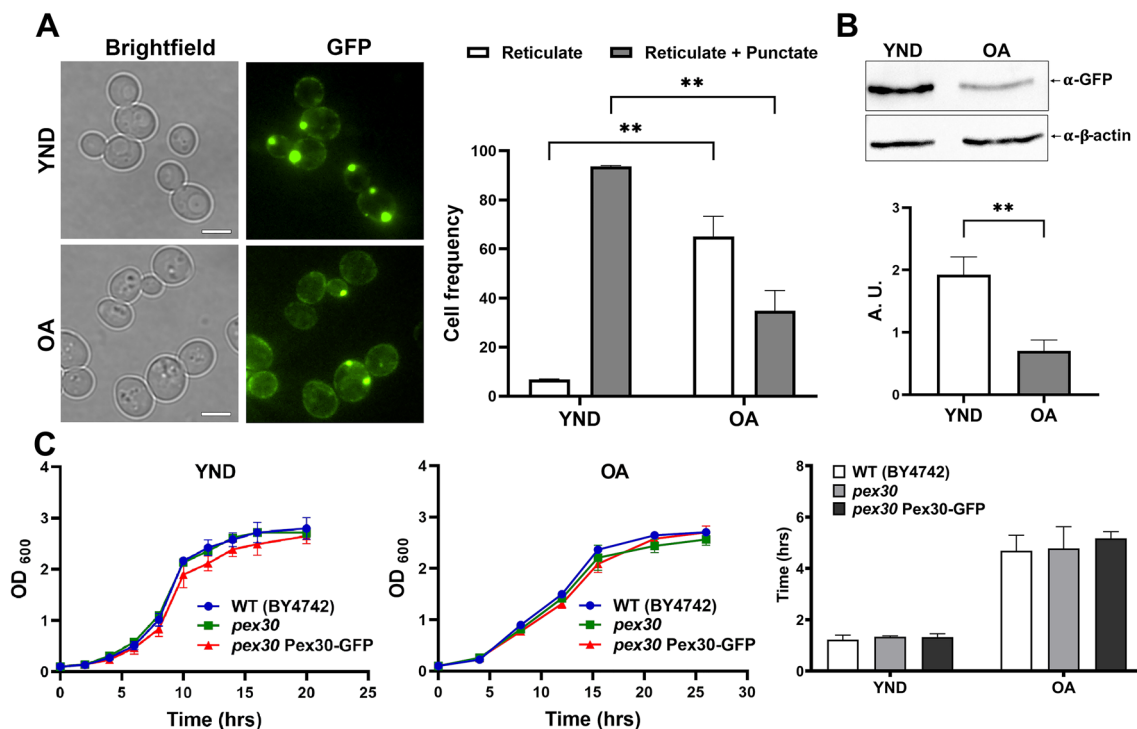


Fig. 1 Expression analysis of GFP tagged Pex30 and its effect on the growth of *pex30*Δ cells. **A** Fluorescence microscopy images of *pex30*Δ cells expressing Pex30-GFP cultured in YND and OA media are depicted. Quantitative analysis of the expression phenotype in YND and OA cultured cells is represented as bar diagrams. Sixty cells were analyzed from each experiment and error bars indicate the SEM from two independent experiments. The significance of the difference between the observed phenotypes was assessed using student's *t* test. Values of $p < 0.01$ were considered as significant (**). **B** Whole cell lysates equivalent to 3 OD₆₀₀ were resolved in a 10% SDS-PAGE gel and protein expression was analyzed by western blot-

ting using an α-GFP antibody. The Pex30-GFP immunoblots were normalized with β-actin for statistical analysis and represented as bar diagrams. Values of $p < 0.01$ were considered as significant (**). **C** The effect of expression of Pex30-GFP on cell growth was assessed by monitoring the growth kinetics of *pex30*Δ, *pex30*Δ cells expressing Pex30-GFP and WT cells. The growth curve was obtained by plotting absorbance (Y axis) against time (X axis). Error bars indicate SEM from two independent experiments. The doubling time of the strains was analyzed and the significance of the difference was determined by using two-way ANOVA (with multiple comparisons)

phenotypes viz. only reticulate and both reticulate and punctate phenotype (Fig. 1A). Quantitative data showed a significant increase in the number of cells exhibiting only reticulate phenotype in OA cultured cells when compared to cells grown in YND (Fig. 1A). Sixty random cells were counted from fluorescence images taken of cells grown in YND and OA from two independent experiments. The percentage of cells exhibiting only reticulate phenotype was 5% in YND media as compared to 72% in OA (Fig. 1A). Our observation is in line with studies that reported ER localization of Pex30 in cells grown in OA (David et al. 2013). Furthermore, the expression of Pex30 in YND and OA was analyzed by western blotting using α-GFP antibody (Fig. 1B). Quantification analysis of the α-GFP probed band showed reduced expression levels of Pex30 in OA. To understand if this altered expression level has any effect on the growth of the cells, WT, *pex30*Δ and *pex30*Δ expressing Pex30-GFP were analyzed for their growth kinetics (Fig. 1C). The doubling time of WT (1.22 h in YND and 4.68 h in OA) *pex30*Δ (1.33 h in

YND and 4.77 h in OA) and *pex30*Δ expressing Pex30-GFP (1.32 h in YND and 5.17 h in OA) did not alter significantly (Fig. 1C).

Purified Pex30 retained its secondary structure

In order to investigate the phosphorylation state of Pex30 and the potential effect of this PTM on the protein, purification of Pex30 was performed by immobilized metal ion affinity chromatography (IMAC). *S. cerevisiae* cells expressing His-tagged Pex30 under the control of an inducible galactose promoter were initially cultured in media containing glucose and raffinose as carbon source. Subsequently, the expression of Pex30 was induced by exposing the cells in raffinose-containing medium to a galactose pulse for 6 h. Protein expression was further confirmed by western blotting using α-His antibody (Fig. 2A). Both SDS-PAGE and western blotting analysis with α-His antibody indicates that

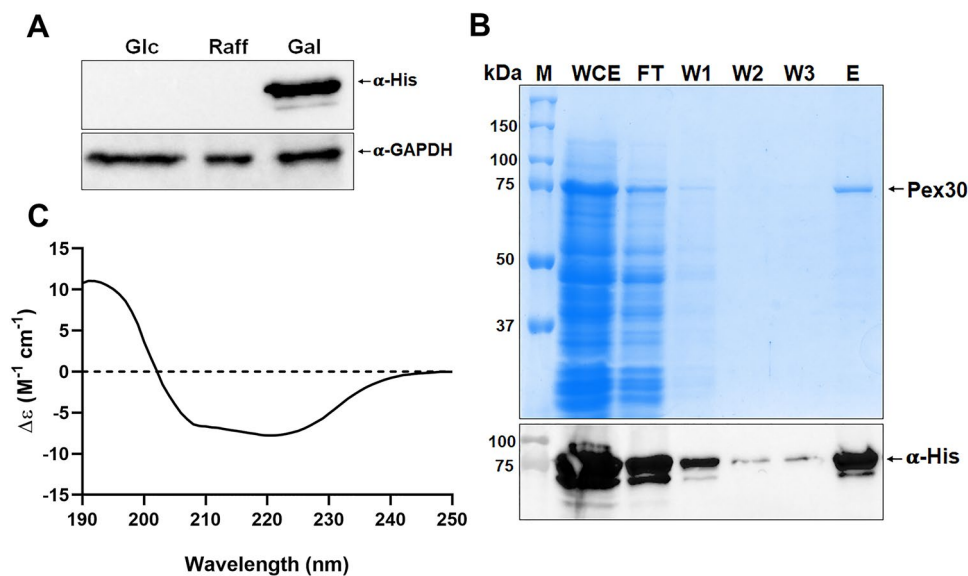


Fig. 2 Expression and structural characterization of His-tagged Pex30. **A** Cells pre-cultured in YND media were subsequently cultured in raffinose followed by induction of the Pex30-His-HA cassette by the addition of galactose. The induced cells were then harvested and lysed using zirconia beads. Protein concentrations were measured by the Bradford protein estimation method and GAPDH was used as a loading control. Samples were run on a 10% SDS-PAGE gel and protein expression was confirmed by western blotting using α -His antibody. **B** represents affinity purification of galactose-induced Pex30 protein under native conditions. Coomassie-stained

10% SDS-PAGE gel depicting purification of His-tagged Pex30 and was confirmed by western blotting using an α -His antibody. *M* protein marker (kDa), *WCE* whole cell extracts, *FT* flow through, *W* wash, *E* elution. **C** Secondary structure determination of Pex30. The purified Pex30 protein was subjected to a desalting column pre-calibrated with 20 mM PB. The desalted protein eluted in PB was then analyzed via far-UV CD spectroscopy followed by *in-silico* analysis using the BeStSel online tool. The CD spectrum for Pex30 was obtained by plotting the wavelength (nm; X axis) against delta epsilon (Y axis)

Pex30 was purified without any contaminating protein bands (Fig. 2B).

Experimental data deciphering the secondary structure of Pex30 has not been reported yet. To explore the possibility of determining the secondary structure of Pex30, the purified protein was desalted and then analyzed by far-UV CD spectroscopy (Fig. 2C). Previous studies have demonstrated the utility of far-UV CD spectroscopy in the successful determination of secondary structure conformations of proteins (Kelly et al. 2005). In far-UV CD spectroscopy, the acquired CD spectrum is directly associated with the folding conformation of the protein. The CD spectrum represents the different secondary structure content like α -helix, β -sheets, turns and random coils that depends on the magnitude and characteristic shape of the spectra (Kelly et al. 2005; Greenfield 2006). Typically, the CD spectrum of an α -helix shows negative peaks at 222 and 208 nm and a positive peak at 193 nm (Greenfield 2006). The obtained data from the far-UV CD spectroscopy of purified Pex30 was analyzed *in silico* by using an online tool, BeStSel, that can predict the folds and secondary structure content of proteins (Micsonai et al. 2015, 2018). Our *in silico* analysis indicates that the purified Pex30 has retained its secondary structure (Fig. 2C) which predominantly comprises of α -helices (51%) followed by a significant proportion of β -sheets (25%) and random

coils (17%) and a minor portion of turns (7%). Recently a computational method that can predict 3D structures of proteins to near experimental accuracy was developed (Jumper et al. 2021). The structure of Pex30 predicted using this method is shown in Supplementary Fig. 1 and primarily comprises of α -helices (Supplementary Fig. 1, (Jumper et al. 2021)).

Pex30 is phosphorylated at Thr60, Ser61 and Ser511

To gain insights into the phosphorylated state of Pex30, a fraction of the obtained Pex30 eluate from purification was treated with CIAP. The mobility of the CIAP treated sample was analyzed in comparison to the untreated sample in a phos-tag SDS-PAGE gel. A phos-tag is a gel additive that selectively binds to the phosphate groups present in a protein molecule and thereby produces a shift in the electrophoretic mobility making it easier for the PTM to be detected in an SDS-PAGE (Kinoshita et al. 2009). The sample incubated with phosphatase (+ CIAP) was observed to have slightly increased migration indicating the removal of phosphate groups from the protein (Fig. 3A, lower panel) whereas no difference in migration patterns of the CIAP treated (+CIAP) and untreated (-CIAP) protein samples

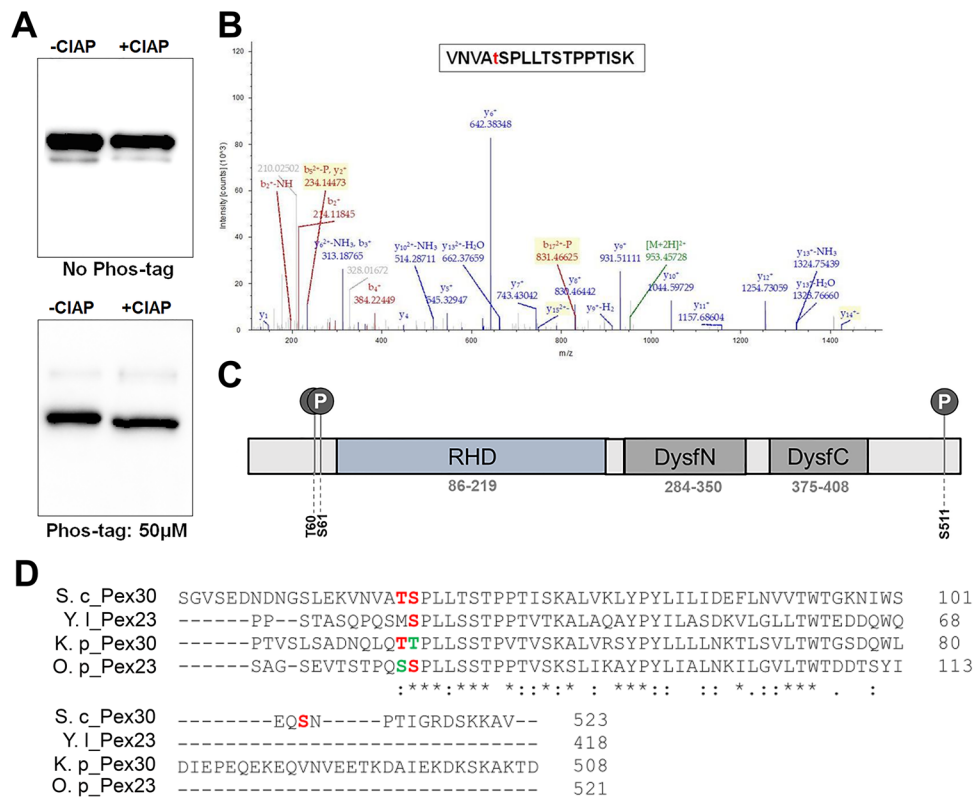


Fig. 3 Pex30 is phosphorylated at three residues in vivo **A** Histagged Pex30 expressed from inducible galactose promoter was affinity purified by the use of Ni/NTA resin and the protein was eluted in tris buffer (pH 7.5). Proteins from CIAP treated and untreated samples were analyzed both by conventional SDS-PAGE and phos-tag SDS-PAGE followed by immunoblotting with α -GFP antibody. **B** Representative MS/MS spectrum depicting phosphorylation of Pex30 at Thr60 (VNVAtSPLLSTPPTISK; m/z 953.500; MH+ : 1905.99309 Da; z = +2). **C** Schematic representation of Pex30 indicating the position of the identified phosphorylation sites. RHD, reticulon homology domain was predicted by using HH-pred (Hildebrand et al. 2009). DysfN/DysfC, N-terminal dysferlin domain and

C-terminal dysferlin domain are represented according to Simple Modular Architecture Research Tool (SMART, ID: SM00693 and SM00694). This is taken from Saccharomyces Genome Database, SGD (<https://www.yeastgenome.org>). **D** Sequence alignment of *S. cerevisiae* Pex30 with its homologues in *Y. lipolytica* (Pex23), *K. phaffii* (Pex30) and *O. polymorpha* (Pex23) illustrating the position of the phosphorylated residues identified in this study. Amino acid residues of *S. cerevisiae* Pex30 highlighted in red indicates the identified phosphorylated residues; the conserved phosphorylated residues in other yeast species are also marked in red. Amino acids highlighted in green indicates the presence of residues that are phosphorylatable but not conserved

were observed in a conventional SDS-PAGE gel (Fig. 3A, upper panel).

To further identify the phosphorylation sites, mass spectrometry was performed on the purified Pex30. Efficient sequence coverage of ~54% was obtained for Pex30 and this included 16 phosphorylation sites reported earlier. However, only two different peptides exhibited a ppm of -0.1 and -0.63 that indicates the presence of additional PTM moiety when compared to the predicted molecular mass for the peptides. Out of the three sites that we have identified with high confidence Thr60, Ser61 have been reported in phosphoproteome studies (Albuquerque et al. 2008; Lanz et al. 2021) and Ser511 has not been reported earlier. The sites with PEP < 0.01 were identified to be phosphorylated (Fig. 3B, C). Further we analyzed if the identified sites are conserved in various yeast species by multiple sequence alignment

using Clustal Omega (Sievers et al. 2011). Of the identified sites, Thr60 is conserved in *S. cerevisiae* and *Komagataella phaffii* whereas Ser61 is conserved in *S. cerevisiae*, *Yarrowia lipolytica* and *Ogataea polymorpha* (Fig. 3D). Thus phos-tag SDS-PAGE and MS analysis data provide evidence for the phosphorylation of Pex30 in vivo.

Mutation of the identified phosphorylated residues to non-phosphorylatable or phosphomimetic variants does not alter the expression of the protein and growth of cells

To explore the functional significance of the identified phosphorylation of Pex30, mutant variants of the protein were generated by exchanging the threonine and serine residues with non-phosphorylatable alanine (A) or phosphomimetic

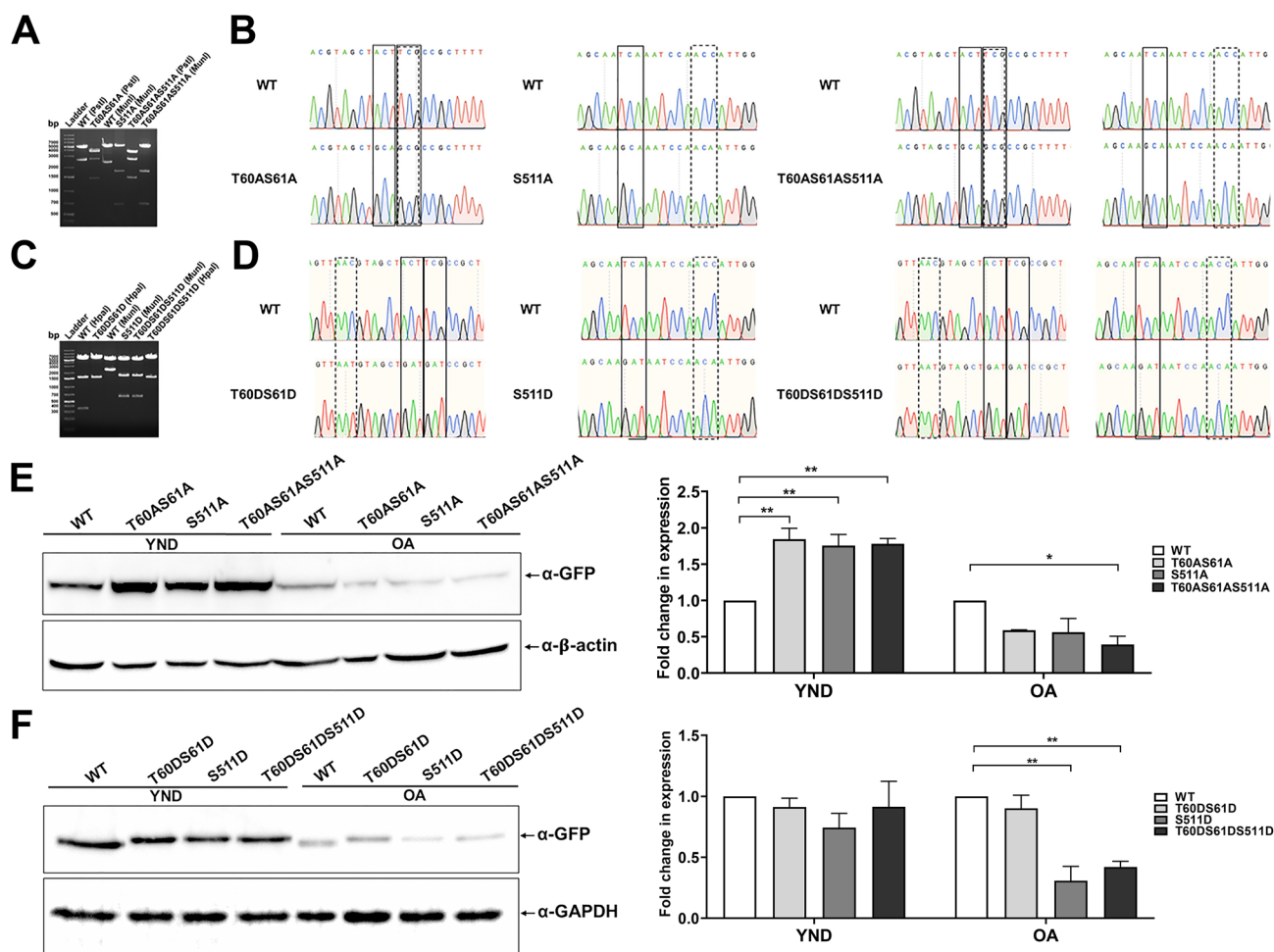


Fig. 4 Site-directed mutagenesis and expression of the mutant variants **A** represents agarose gel images showing restriction digestion profiles to confirm the presence of PCR amplified clones carrying the non-phosphorylatable mutation (left). Site-directed mutagenesis was performed by changing the phospho-sites to non-phosphorylatable alanine. **B** The mutations were further confirmed by sequencing analysis. The solid line boxes indicate the desired mutations and the dotted boxes denotes alteration in nucleotide without changing the amino acid to generate a unique restriction site for screening of mutants. Boxes in both solid and dotted line denote the formation of unique restriction sites while generating mutations in the phosphorylated residues. **C** and **D** represent restriction digestion (left) and sequencing analysis (right) performed to screen and confirm the mutants in which the phospho-sites were exchanged with the amino acid aspartate to generate phosphomimetic variants of Pex30. **E** represents expression analysis of the non-phosphorylatable mutants grown in YND and OA medium. Whole cell lysates corresponding to 3 OD₆₀₀ units were resolved by SDS-PAGE and probed with α -GFP antibody. For

quantitative analysis, the GFP blots were normalized with β -actin as a loading control and represented as bar diagrams. The error bars indicate SEM obtained from two independent experiments (right). A two-way ANOVA with multiple comparisons was used to determine the significance of difference between the expression levels of WT Pex30 and the non-phosphorylatable mutants. Values of $P < 0.05$ were considered significant (*) and $P < 0.01$ very significant (**). **F** depicts expression analysis of the phosphomimetic mutants. 3 OD₆₀₀ units of whole cell lysates were separated by using SDS-PAGE followed by western blotting with α -GFP antibody (left). Quantitative analysis of the immunoblots was performed by normalizing with GAPDH (loading control) and represented as bar diagrams. Error bars denote SEM obtained from two independent experiments (right). The significance of the difference between the expression levels of WT Pex30 and the phosphomimetic mutants were statistically determined by using two-way ANOVA (with multiple comparisons). Values of $P < 0.05$ were considered significant (*) and $P < 0.01$ very significant (**)

aspartic acid (D). Due to the close proximity of the residues Thr60 and Ser61, we generated a variant in which both the phosphorylated sites were changed. Ser511 was also changed to either A or D to create a single mutant variant of the protein. Moreover, a mutant strain with all the three identified sites exchanged with A or D was also generated.

The confirmation of all the mutant variants of Pex30 was achieved by restriction digestion with specific enzymes (Fig. 4A, C) and DNA sequencing of the constructs (Fig. 4B, D). The mutant variants were then introduced into *pex30* Δ cells. The protein expression levels of the mutants were analyzed and compared to that of the WT protein via western

blotting using an α -GFP antibody (Fig. 4E, F). The change in protein expression levels was quantified and is represented as a fold change in expression. In cells cultured in the YND medium, the non-phosphorylatable mutants exhibited significant increase in protein expression in comparison to the WT protein whereas in OA growth conditions, reduced protein expression was observed in cells bearing T60AS61AS511A mutation (Fig. 4E). In addition, protein expression levels of the phosphomimetic mutants were unaltered in YND but cells bearing S511D and T60DS61DS511D mutations displayed a significant reduction in protein expression in OA (Fig. 4F). Strikingly, a small shift in the band of the phosphomimetic mutants was observed in comparison to WT in both YND and OA (Fig. 4F). This change could be due to the

change of the overall charge which may affect the electrophoretic mobility of the protein and probable conformational changes in the native structure of Pex30 due to amino acid substitution resulting in a small increase in molecular weight (Fig. 4E). Similar decreased electrophoretic mobility upon substitution of aspartate with serine was also reported earlier (Léger et al. 1997). This distinct band shift was not observed in the non-phosphorylatable mutants.

Fluorescence microscopy analysis revealed no significant difference between the distribution and expression of the mutant variants and WT protein (Fig. 1A). Cells expressing both the non-phosphorylatable and phosphomimetic mutant variants exhibited the typical punctate as well as reticulate phenotype as exhibited by WT Pex30 when grown in YND

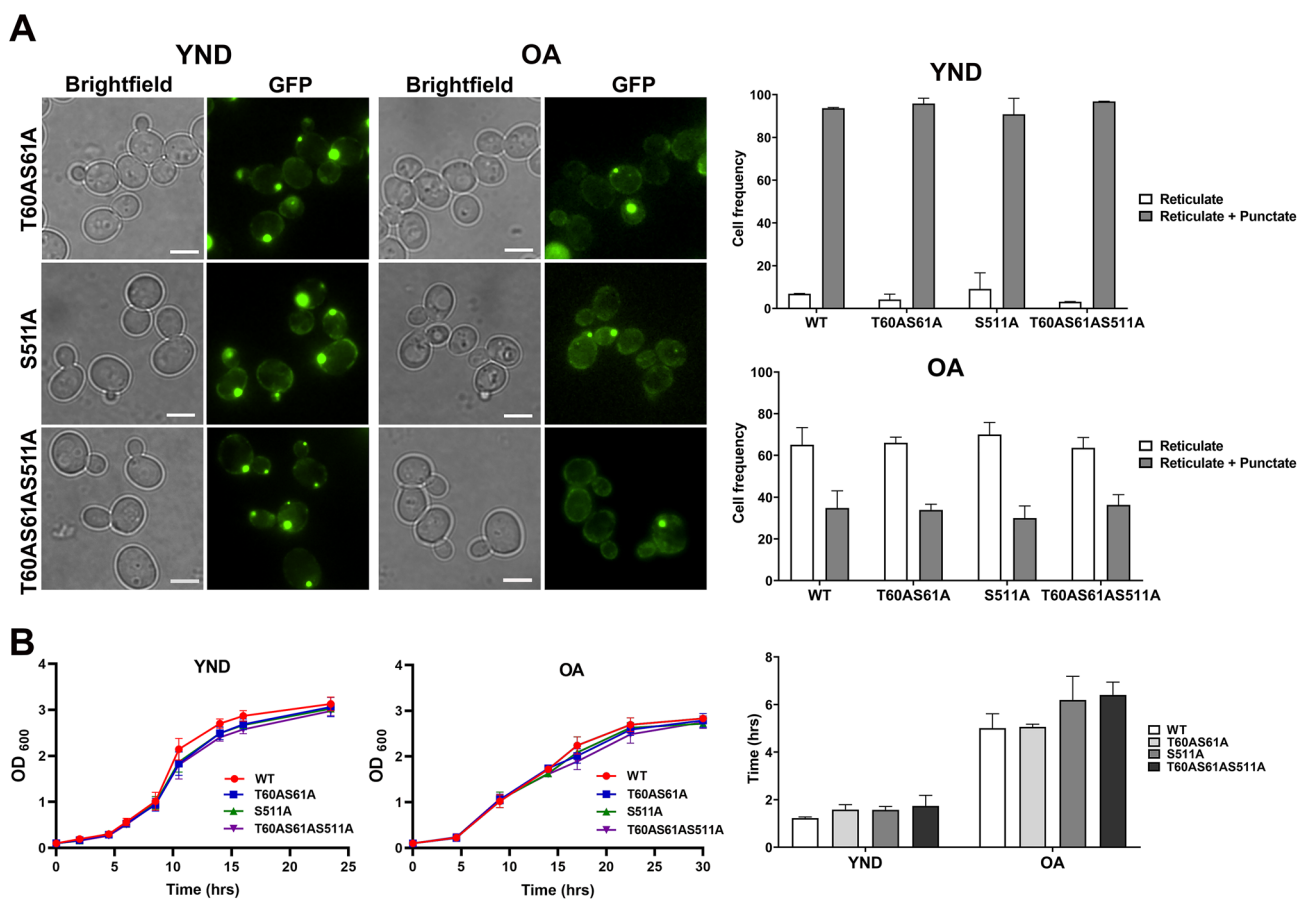


Fig. 5 Microscopy analysis of cells expressing the non-phosphorylatable variants of Pex30 and effect on cell growth. **A** Fluorescence microscopy images of *pex30*Δ cells expressing the GFP-tagged non-phosphorylatable variants of Pex30 (T60AS61A, S511A and T60AS61AS511A). Cells were grown in both YND and peroxisome inducing OA media incubated at 30 °C. A group of 3–4 cells exhibiting GFP fluorescence from each mutant strain is represented with the corresponding brightfield images. Scale bar represents 5 μm. Quantitative analysis of phenotype exhibited by YND and OA cultured cells is represented as bar diagrams. 60 cells from each experiment were analyzed. Error bars indicate SEM from two independent experi-

ments. The statistical significance was determined by using two-way ANOVA with multiple comparisons. **B** The effect of expression of the non-phosphorylatable Pex30 mutants on yeast cell growth was determined by plotting a growth curve. Yeast cells were cultured both on YND (left) and OA media (middle) and the growth kinetics was assessed by measuring the optical density of cells at 600 nm (OD_{600}) over the indicated time. The doubling time of the yeast strains was measured by calculating difference in growth rates during the exponential phase (right). Error bars indicate SEM calculated from two independent experiments. The statistical significance was determined by using two-way ANOVA with multiple comparisons

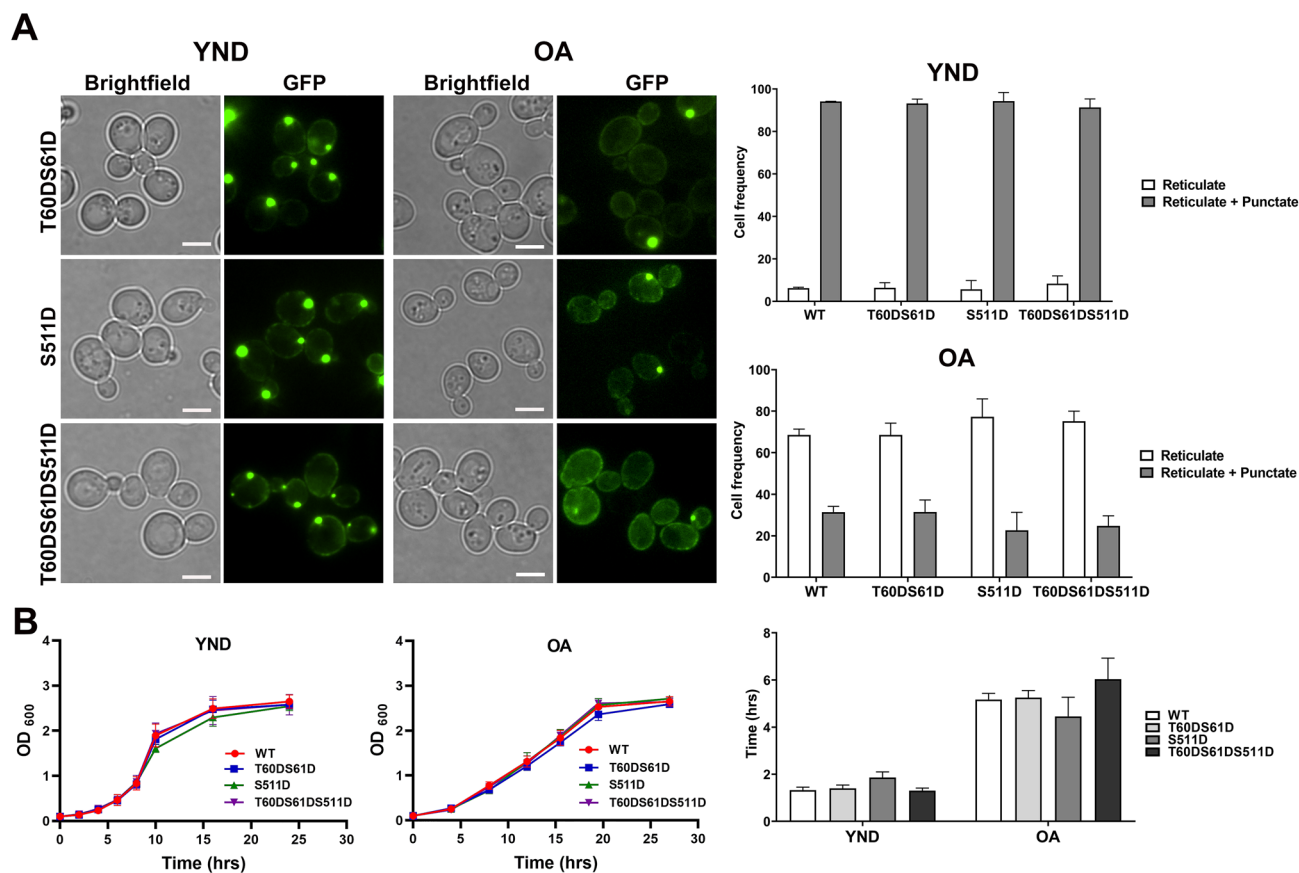


Fig. 6 Microscopy analysis of the cells expressing phosphomimetic variants of Pex30 and effect on cell growth. **A** Fluorescence microscopy images of pex30Δ cells expressing the GFP-tagged phosphomimetic variants of Pex30 (T60DS61D, S511D and T60DS61DS511D). Cells were grown in both YND and OA media. A group of 3–4 cells exhibiting GFP fluorescence from each mutant strain is represented with the corresponding brightfield images. Scale bar represents 5 μm. Quantitative analysis of phenotype exhibited by YND and OA cultured cells is represented as bar diagrams. 60 cells from each experiment were analyzed. Error bars indicate SEM from two independent experiments. The statistical significance was determined by

and OA media (Figs. 5A, 6A). Quantification of fluorescence images of these cells also revealed a phenotype comparable to the cells expressing WT Pex30 in YND and OA. Quantitative analysis revealed that most cells grown in YND media exhibited punctate plus reticulate phenotype whereas in OA cultured cells, in addition to this, cells with only reticulate phenotype were also observed. The growth kinetics of yeast cells transformed with the mutant variants and WT Pex30 was monitored. The growth rate of the mutant strains and doubling time did not differ significantly when compared to cells expressing WT Pex30 in both the growth conditions (Figs. 5B, 6B).

using two-way ANOVA with multiple comparisons. **B** The effect of expression of the phosphomimetic mutants on yeast cell growth was determined by plotting a growth curve. Yeast cells were cultured both on YND (left) and OA media (middle) and the growth kinetics was assessed by measuring the optical density of cells at 600 nm (OD₆₀₀) over the indicated time. The doubling time of the yeast strains was measured by calculating the difference in growth rates during the exponential phase (right). Error bars indicate SEM calculated from two independent experiments. The statistical significance was determined by using two-way ANOVA with multiple comparisons

Mutations in the phosphorylation sites did not alter the localization of the protein

To investigate if the mutant variants exhibit altered subcellular localization, they were co-transformed with plasmids that specifically label peroxisomes or ER. Microscopy analysis revealed that the puncta-like phenotype of WT Pex30 localizes in close proximity to peroxisomes, and in some cells, the GFP puncta were observed to partially co-localize with peroxisomes (Fig. 7A, B). The association between Pex30 puncta and peroxisomes was also analyzed by measuring the fluorescence intensity and is represented as intensity line profiles (Fig. 7A, B). This observation is in line with an earlier study by David and colleagues, where the authors suggest that a small portion of Pex30 targets to peroxisomes

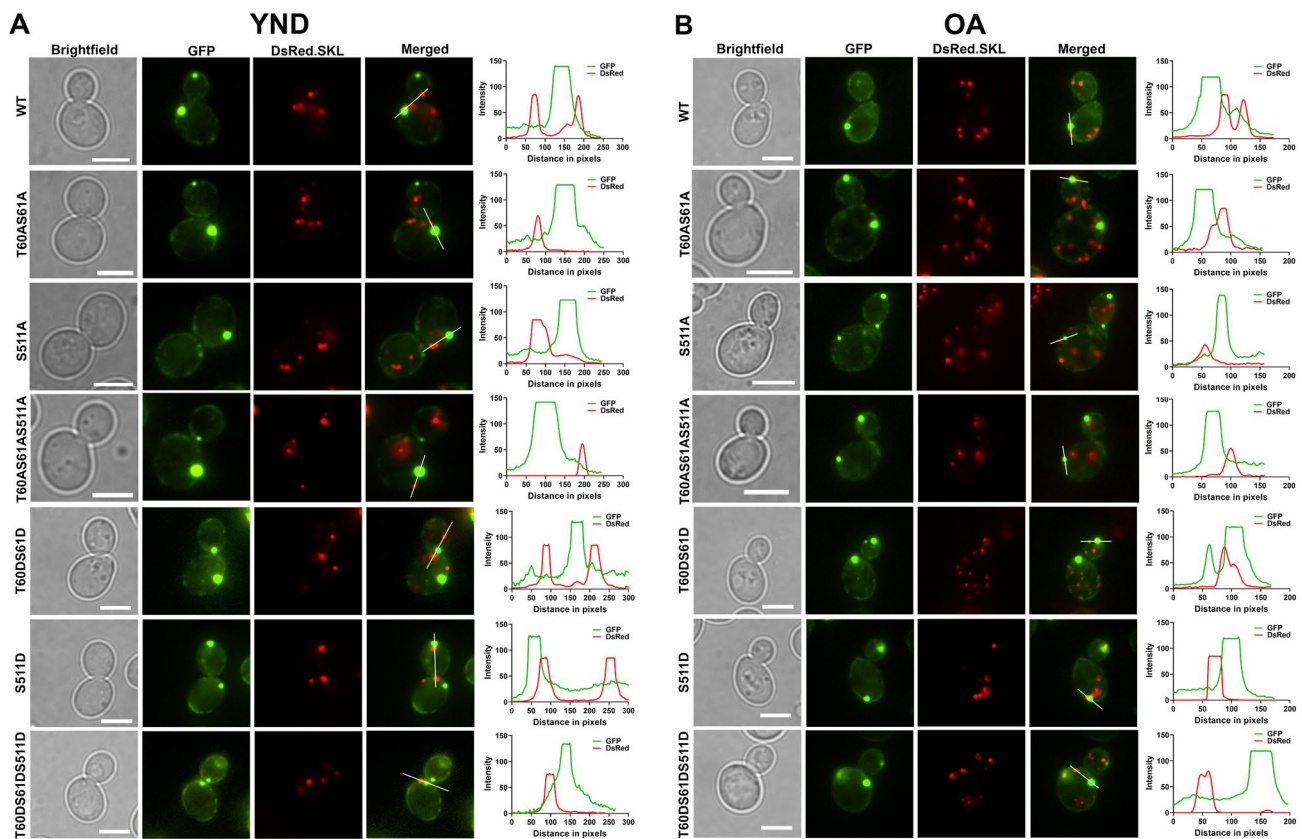


Fig. 7 Mutant variants of Pex30 do not show altered localization to peroxisomes. Pex30 Δ cells consisting of the GFP expressing non-phosphorylatable and phosphomimetic variants of Pex30 was co-transformed with a plasmid containing DsRed.SKL, which specifically targets to peroxisomes. The cells were cultured in YND media (A) and OA (B) and subsequently co-localization of GFP puncta with

DsRed.SKL marked peroxisomes were analyzed by fluorescence microscopy. The extent of co-localization was analyzed by intensity profiles obtained from the regions (line) depicted in the merged panel and is illustrated as graphs. The fluorescence intensity of the green and red fluorophores was measured using ImageJ. Scale bar represents 5 μ m

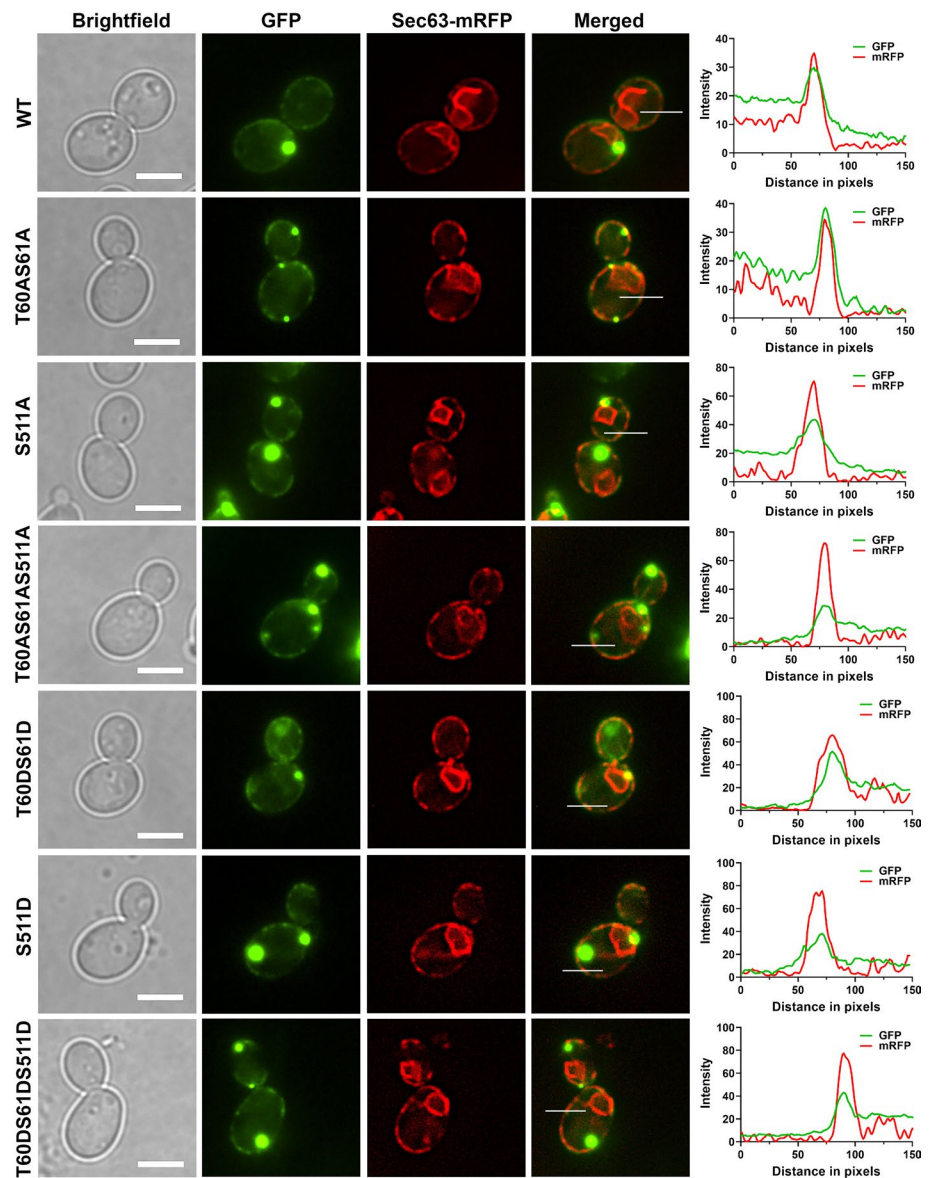
and the accumulation of peroxisomes is juxtaposed to Pex30 puncta (David et al. 2013). As observed in WT cells, both the non-phosphorylatable and phosphomimetic variants of Pex30 displayed similar colocalization with DsRed.SKL marked peroxisomes which indicates that targeting of Pex30 was not altered in the mutant variants (Fig. 7A, B). The targeting of WT Pex30 and mutant variants to ER was analyzed by co-expressing Sec63-mRFP. As reported earlier (David et al. 2013; Joshi et al. 2016), our data also indicates that the reticulate structure of WT Pex30 and the mutant variants colocalizes mostly with the cortical ER at the cell periphery (Fig. 8). This suggests that phosphorylation of Pex30 at Thr60, Ser61 and Ser511 most likely is not involved in its targeting to peroxisomes and the ER.

Peroxisome phenotype in mutant variants of Pex30

To assess whether the non-phosphorylatable and phosphomimetic mutations influence the number of peroxisomes in yeast cells, we analyzed the total number of peroxisomes

per cell in the mutant strains cultured in both YND and OA media (Fig. 9). Cells expressing WT Pex30 showed a clear induction of peroxisomes when grown in OA media (10.1 ± 3.4 versus 5.9 ± 2.2). In YND, cells bearing non-phosphorylatable mutant variants of Pex30 viz. T60AS61A and T60AS61AS511A displayed a similar number of peroxisomes as in cells expressing WT Pex30 (6.15 ± 2.0 and 5.5 ± 1.5); whereas the number of peroxisomes decreased in cells bearing S511A mutation (5.1 ± 2.3). Similarly, the phosphomimetic variants T60DS61D and T60DS61DS511D exhibited a peroxisome number similar to the WT (5.8 ± 2.5 and 5.6 ± 2.4); whereas a decrease in peroxisome number was observed in the S511D phosphomimetic mutant (4.9 ± 1.9). Upon growth in OA containing media, cells expressing non-phosphorylatable variants T60AS61A and T60AS61AS511A exhibited a similar number of peroxisomes (9.7 ± 3.3 and 10.5 ± 3.3) as compared to cells expressing the WT version of the protein (10.1 ± 3.4); whereas a decrease in peroxisome number was observed in the S511A mutant variant (8.9 ± 2.9). Notably,

Fig. 8 Mutant variants of Pex30 do not show altered localization to ER. Pex30 Δ cells containing the GFP expressing non-phosphorylatable and phosphomimetic variants were co-transformed with the plasmid containing Sec63-mRFP, which specifically targets to ER. The cells were cultured in YND media and subsequently co-localization of the Pex30-GFP with Sec63-mRFP marked ER was analyzed by fluorescence microscopy. The extent of co-localization was analyzed by intensity profiles obtained from the regions (line) depicted in the merged panel and is illustrated as graphs. The fluorescence intensity of the green and red fluorophores was measured using ImageJ. Scale bar represents 5 μ m



in peroxisome inducing OA media, all the phosphomimetic variants of Pex30, i.e., T60DS61D, S511D and T60DS61DS511D displayed a decrease in peroxisome number (7.7 ± 2.8 , 7.8 ± 3.2 and 7.3 ± 2.5). Hence, our data indicate that mutation at S511 results in decrease of peroxisome number in both YND and OA growth conditions. In addition, under peroxisome proliferating growth conditions, the phosphomimetic variants of Pex30 exhibit a negative effect on the proliferation of peroxisomes.

Discussion

Pex30 is an intriguing protein whose role in peroxisome biogenesis is not fully understood. However, convincing data suggest the enrichment of Pex30 at specific sites of the

ER and a role for this in the formation of PPVs that go on to form mature peroxisomes (Wang et al. 2018; Joshi et al. 2016). Interestingly, loss of Pex30 was also reported to result in an increase in the number of peroxisomes in *S. cerevisiae* (Vizeacoumar et al. 2004; David et al. 2013). In line with this David and colleagues also showed that the formation of peroxisomes from ER is more efficient in the absence of Pex30. Deletion of Pex30 in cells lacking Pex11 (reduced number of peroxisomes) which are blocked in peroxisome fission, resulted in restoration of the peroxisome number to WT levels (David et al. 2013). On the contrary, the rate of formation of new peroxisomes was reported to decrease in cells devoid of Pex30 (Joshi et al. 2016). The experimental set up used in both the above-mentioned papers may be a reason for this discrepancy observed.

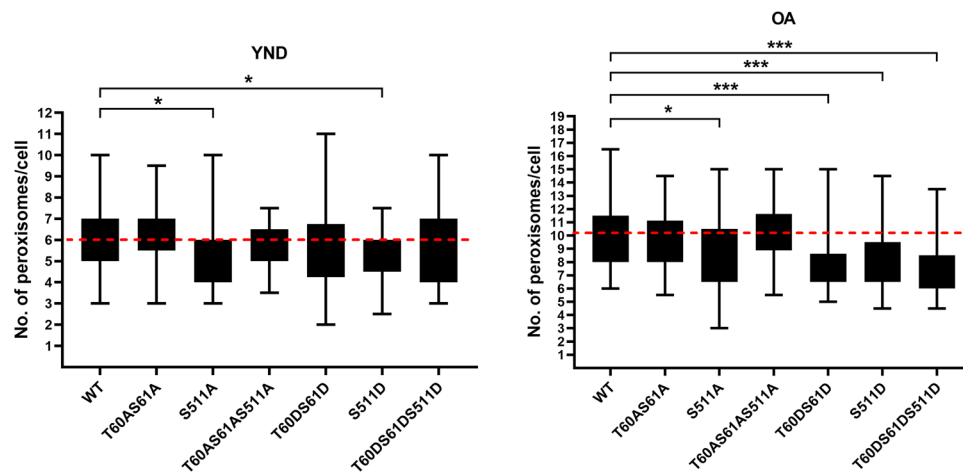


Fig. 9 Mutant variants of Pex30 exhibit altered peroxisome number. WT and mutant variants of Pex30 expressing the peroxisomal marker DsRed.SKL were analyzed for peroxisome number. For quantification of peroxisome number, yeast strains were cultured in both YND and peroxisome inducing OA media. For each yeast strain, peroxisomes were counted by merging the Z stack and 40 cells were counted from

one independent experiment. The data represented is from two such experiments. The box and whisker plot illustrates the diversity of peroxisome number among the yeast strains. The red dashed line denotes the average (mean) number of peroxisomes in WT cells. Values of $P < 0.05$ were considered significant (*), $P < 0.01$ very significant (**), and $P < 0.001$ extremely significant (***)

In this study, we have successfully expressed and purified the full-length Pex30 and structural determination using CD showed that the secondary structure conformation of the purified protein was retained. Analysis of CD data shows that Pex30 has predominantly α -helices followed by β -sheets. At the N-terminus of the protein a reticulon-homology domain that is predominantly α -helical has been predicted. The dysferlin domain in this protein is conserved and is ubiquitously present in other proteins belonging to this family (Sula et al. 2014). β -sheet structure for this domain in human dysferlin has been reported (Sula et al. 2014). Analysis of the Pex30 structure obtained from AlphaFold also shows a β -sheet structure for this domain. Interestingly, no role for this domain in the interaction of the protein with Pex28, Pex29 and Pex32 has been reported. Cells expressing Pex30 lacking dysferlin-domain show a peroxisome phenotype similar to that of *pex30* Δ cells (Ferreira and Carvalho 2021).

The expression of Pex30 was observed to decrease in cells grown in the OA medium in our study. This is unlike as reported earlier where the authors have used a gal inducible expression system (David et al. 2013). However, earlier data also highlighted the role of Pex30 as a negative regulator of peroxisomes (Vizeacoumar et al. 2004). OA is a peroxisome-inducing medium and reduced Pex30 may regulate this increase in peroxisome number. Interestingly, this reduction in expression was also accompanied by a change in distribution pattern of the protein to mostly reticular distribution in OA. However, if the reduced expression is solely responsible for this needs to be investigated. Increased expression of Pex30 in the non-phosphorylatable mutants was observed in YND grown cells. This could be due to altered interactions

with proteins such as Pex28, Pex29 and Pex32. Recent study by Ferreira and Carvalho also reported that partial deletions of Pex30 RHD resulted in lower steady-state levels of Pex30 as well as its partners Pex28, Pex29, and Pex32 (Ferreira and Carvalho 2021). It can be envisaged that the mutations may change interactions of the protein and thereby stabilize the protein and result in increased expression. Whole proteome studies have identified several residues that are most likely sites for phosphorylation. In this work we have shown that *S. cerevisiae* Pex30 is phosphorylated at three residues Thr60, Ser61 and Ser511. Thr60, Ser61 are present in the N-terminal of the protein and Ser511 is at the extreme C-terminus of the protein. Out of the three residues identified to be phosphorylated Ser511 is unique to *S. cerevisiae*. Interestingly, the number of Pex30 protein family members and the effect of lack of these proteins varies in different yeast species. Paralogs of Pex30 are identified in *S. cerevisiae*. A role for these proteins in various routes of regulation of peroxisome number has been hypothesized. Hence, it may be hypothesized that Ser511 may be unique to *S. cerevisiae* and may be needed for its specific interactions. We further replaced the identified residues with non-phosphorylatable or phosphomimetic residues and analyzed for variations in protein expression, peroxisome phenotype and the localization of mutant variants to peroxisomes and ER. Our data demonstrates that both non-phosphorylatable and phosphomimetic variants behave similarly like the WT protein. This led us to conclude that phosphorylation most likely does not play an important role in the localization of the protein to peroxisomes or ER. Other cellular mechanisms may be needed for this targeting. Identifying the domains

of the protein that particularly interact with proteins on the peroxisomes/ER may help understand this mechanism.

Interestingly, peroxisome number in cells cultured in YND and OA did not alter significantly in non-phosphorylated variants, except for the Ser511A, which showed a reduced number in OA. Reduced number of peroxisomes in peroxisome-inducing growth conditions was observed when the residues were replaced with phosphomimetic aspartate residue. A role for Pex30 in regulating the membrane contact sites of ER and peroxisomes has been reported. Change in the phosphorylation status in the mutants studied may result in altered membrane contact sites and thereby affect the number of peroxisomes. Earlier studies have reported an increase in peroxisome number when the C-terminus of the protein including C-Dysferlin domain was deleted (David et al. 2013). S511 lies in the domain of unknown function and the dysferlin domain in cells expressing the mutant variant (S511A and S511D) is intact and hence no increase in peroxisome number was observed. Interestingly, Ser511 which is not conserved among other yeast species depicted altered peroxisome number upon changing to non-phosphorylatable or phosphomimetic variant. One hypothesis could be that these mutants may be differentially affected in their interaction with interacting proteins. Phosphorylation and dephosphorylation cycle may be needed for successive interactions of the protein to accomplish its function. Further experiments that will decipher the role of phosphorylation in interaction with proteins and lipids may shed more light on this. A role for phosphorylation in the formation of higher-order structures of the protein or to make distinct protein interactions required to regulate peroxisome biogenesis can be envisaged.

Our data demonstrates that phospho-mimicking mutant variants of *S. cerevisiae* Pex30 result in altered number of peroxisomes. This suggests that phosphorylation of Pex30 may play a vital role in regulating peroxisome number and does not influence the localization of the protein to ER and peroxisomes. Interestingly, an important role for Pex30 in lipid droplet biogenesis has also been shown. Pex30 has been proposed to function as an adapter at the ER-peroxisome and ER-lipid droplet contact sites (Ferreira and Carvalho 2021). Different Pex30 complexes have been identified that are unique for the interaction and formation of membrane contact sites with peroxisomes and lipid droplets. Future studies in this regard can decipher Pex30 interactions regulated by this PTM and the role of this modification in biogenesis of these organelles.

Though several peroxisomal proteins are identified to be phosphorylated by whole proteome approaches, not many validation studies have been performed (Infant et al. 2021). It is therefore important to study the functional relevance and decipher the molecular details that governs this regulatory mechanism.

Supplementary Information The online version contains supplementary material available at <https://doi.org/10.1007/s00438-022-01872-8>.

Author contributions NMD: performed the experiments, wrote the first draft of the manuscript and prepared the figures. TI and PKS: performed experiments. RPT and SN: conceived the idea and analyzed the data. SN: edited the manuscript and procured funding. All authors read and approved the final manuscript.

Funding This work was supported by the Department of Biotechnology (DBT), Government of India [BT/PR25097/NER/95/1013/2017] and Top-up of Start-Up grant from IIT Guwahati.

Availability of data and materials Not applicable.

Code availability Not applicable.

Declarations

Conflict of interest The authors declare that they have no conflict of interest.

Ethical approval This article does not contain any studies with human participants or animals performed by any of the authors.

References

- Akşit A, van der Klei IJ (2018) Yeast peroxisomes: how are they formed and how do they grow? *Int J Biochem Cell Biol* 105:24–34. <https://doi.org/10.1016/j.biocel.2018.09.019>
- Albuquerque CP, Smolka MB, Payne SH, Bafna V, Eng J, Zhou H (2008) A multidimensional chromatography technology for in-depth phosphoproteome analysis. *Mol Cell Proteomics* 7:1389–1396. <https://doi.org/10.1074/mcp.M700468-MCP200>
- Baerends RJ, Faber KN, Kram AM, Kiel JA, van der Klei IJ, Veenhuis M (2000) A stretch of positively charged amino acids at the N terminus of Hansenula polymorpha Pex3p is involved in incorporation of the protein into the peroxisomal membrane. *J Biol Chem* 275:9986–9995. <https://doi.org/10.1074/jbc.275.14.9986>
- Balta E-A, Wittmann M-T, Jung M, Sock E, Haerberle BM, Heim B, von Zweydford F, Heppt J, von Wittgenstein J, Gloeckner CJ, Lie DC (2018) Phosphorylation modulates the subcellular localization of SOX11. *Front Mol Neurosci*. <https://doi.org/10.3389/fnmol.2018.00211>
- Cohen P (2002) The origins of protein phosphorylation. *Nat Cell Biol* 4:E127–E130. <https://doi.org/10.1038/ncb0502-e127>
- David C, Koch J, Oeljeklaus S, Laernsack A, Melchior S, Wiese S, Schummer A, Erdmann R, Warscheid B, Brocard C (2013) A combined approach of quantitative interaction proteomics and live-cell imaging reveals a regulatory role for endoplasmic reticulum (ER) reticulon homology proteins in peroxisome biogenesis. *Mol Cell Proteom* 12:2408–2425. <https://doi.org/10.1074/mcp.M112.017830>
- Deb R, Nagotu S (2017) Versatility of peroxisomes: an evolving concept. *Tissue Cell* 49:209–226. <https://doi.org/10.1016/j.tice.2017.03.002>
- Deori NM, Kale A, Maurya PK, Nagotu S (2018) Peroxisomes: role in cellular ageing and age related disorders. *Biogerontology* 19:303–324. <https://doi.org/10.1007/s10522-018-9761-9>

- Ferreira JV, Carvalho P (2021) Pex30-like proteins function as adaptors at distinct ER membrane contact sites. *J Cell Biol* 220:e202103176. <https://doi.org/10.1083/jcb.202103176>
- Gietz RD, Sugino A (1988) New yeast-Escherichia coli shuttle vectors constructed with in vitro mutagenized yeast genes lacking six-base pair restriction sites. *Gene* 74:527–534. [https://doi.org/10.1016/0378-1119\(88\)90185-0](https://doi.org/10.1016/0378-1119(88)90185-0)
- Greenfield NJ (2006) Using circular dichroism spectra to estimate protein secondary structure. *Nat Protoc* 1:2876–2890. <https://doi.org/10.1038/nprot.2006.202>
- Haridhasapavalan KK, Sundaravadevelu PK, Bhattacharyya S, Ranjan SH, Raina K, Thummer RP (2021) Generation of cell-permeant recombinant human transcription factor GATA4 from *E. coli*. *Bioproc Biosyst Eng* 44:1131–1146. <https://doi.org/10.1007/s00449-021-02516-8>
- Hildebrand A, Remmert M, Biegert A, Söding J (2009) Fast and accurate automatic structure prediction with HHpred. *Proteins* 77(Suppl 9):128–132. <https://doi.org/10.1002/prot.22499>
- Hunter T (2012) Why nature chose phosphate to modify proteins. *Philos Trans R Soc Lond Ser B Biol Sci* 367:2513–2516. <https://doi.org/10.1098/rstb.2012.0013>
- Infant T, Deb R, Ghose S, Nagotu S (2021) Post-translational modifications of proteins associated with yeast peroxisome membrane: an essential mode of regulatory mechanism. *Genes Cells* 00:1–18. <https://doi.org/10.1111/gtc.12892>
- Johnson LN, Barford D (1993) The effects of phosphorylation on the structure and function of proteins. *Annu Rev Biophys Biomol Struct* 22:199–232. <https://doi.org/10.1146/annurev.bb.22.060193.001215>
- Joshi S, Agrawal G, Subramani S (2012) Phosphorylation-dependent Pex11p and Fis1p interaction regulates peroxisome division. *Mol Biol Cell* 23:1307–1315. <https://doi.org/10.1091/mbc.E11-09-0782>
- Joshi AS, Huang X, Choudhary V, Levine TP, Hu J, Prinz WA (2016) A family of membrane-shaping proteins at ER subdomains regulates pre-peroxisomal vesicle biogenesis. *J Cell Biol* 215:515–529. <https://doi.org/10.1083/jcb.201602064>
- Joshi AS, Nebenfuhr B, Choudhary V, Satpute-Krishnan P, Levine TP, Golden A, Prinz WA (2018) Lipid droplet and peroxisome biogenesis occur at the same ER subdomains. *Nat Commun* 9:2940. <https://doi.org/10.1038/s41467-018-05277-3>
- Jumper J, Evans R, Pritzel A, Green T, Figurnov M, Ronneberger O, Tunyasuvunakool K, Bates R, Židek A, Potapenko A, Bridgland A, Meyer C, Kohl SAA, Ballard AJ, Cowie A, Romera-Paredes B, Nikolov S, Jain R, Adler J, Back T, Petersen S, Reiman D, Clancy E, Zielinski M, Steinegger M, Pacholska M, Berghammer T, Bodenstein S, Silver D, Vinyals O, Senior AW, Kavukcuoglu K, Kohli P, Hassabis D (2021) Highly accurate protein structure prediction with AlphaFold. *Nature* 596:583–589. <https://doi.org/10.1038/s41586-021-03819-2>
- Kelly SM, Jess TJ, Price NC (2005) How to study proteins by circular dichroism. *BBA-Proteins Proteomics* 1751:119–139. <https://doi.org/10.1016/j.bbapap.2005.06.005>
- Kinoshita E, Kinoshita-Kikuta E, Koike T (2009) Separation and detection of large phosphoproteins using Phos-tag SDS-PAGE. *Nat Protoc* 4:1513–1521. <https://doi.org/10.1038/nprot.2009.154>
- Knoblach B, Rachubinski RA (2010) Phosphorylation-dependent activation of peroxisome proliferator protein PEX11 controls peroxisome abundance. *J Biol Chem* 285:6670–6680. <https://doi.org/10.1074/jbc.M109.094805>
- Kunau W-H, Dommes V, Schulz H (1995) β -Oxidation of fatty acids in mitochondria, peroxisomes, and bacteria: a century of continued progress. *Prog Lipid Res* 34:267–342. [https://doi.org/10.1016/0163-7827\(95\)00011-9](https://doi.org/10.1016/0163-7827(95)00011-9)
- Kuravi K, Nagotu S, Krikken AM, Sjollem K, Deckers M, Erdmann R, Veenhuis M, van der Klei IJ (2006) Dynamamin-related proteins Vps1p and Dnm1p control peroxisome abundance in *Saccharomyces cerevisiae*. *J Cell Sci* 119:3994–4001. <https://doi.org/10.1242/jcs.03166>
- Lanz MC, Yugandhar K, Gupta S, Sanford EJ, Faça VM, Vega S, Joiner AMN, Fromme JC, Yu H, Smolka MB (2021) In-depth and 3-dimensional exploration of the budding yeast phosphoproteome. *EMBO Rep* 22:e51121. <https://doi.org/10.15252/embr.202051121>
- Léger J, Kempf M, Lee G, Brandt R (1997) Conversion of serine to aspartate imitates phosphorylation-induced changes in the structure and function of microtubule-associated protein Tau*. *J Biol Chem* 272:8441–8446. <https://doi.org/10.1074/jbc.272.13.8441>
- Lowry O, Rosebrough N, Farr AL, Randall R (1951) Protein measurement with the folin phenol reagent. *J Biol Chem* 193:265–275. [https://doi.org/10.1016/S0021-9258\(19\)52451-6](https://doi.org/10.1016/S0021-9258(19)52451-6)
- Mast FD, Jamakhandi A, Saleem RA, Dilworth DJ, Rogers RS, Rachubinski RA, Aitchison JD (2016) Peroxis Pex30 and Pex29 dynamically associate with reticulons to regulate peroxisome biogenesis from the endoplasmic reticulum. *J Biol Chem* 291:15408–15427. <https://doi.org/10.1074/jbc.M116.728154>
- Metzger MB, Maurer MJ, Dancy BM, Michaelis S (2008) Degradation of a cytosolic protein requires endoplasmic reticulum-associated degradation machinery. *J Biol Chem* 283:32302–32316. <https://doi.org/10.1074/jbc.M806424200>
- Micsonai A, Wien F, Kernya L, Lee YH, Goto Y, Réfrégiers M, Kardos J (2015) Accurate secondary structure prediction and fold recognition for circular dichroism spectroscopy. *Proc Natl Acad Sci USA* 112:E3095–3103. <https://doi.org/10.1073/pnas.1500851112>
- Micsonai A, Wien F, Bulyáki É, Kun J, Moussong É, Lee YH, Goto Y, Réfrégiers M, Kardos J (2018) BeStSel: a web server for accurate protein secondary structure prediction and fold recognition from the circular dichroism spectra. *Nucleic Acids Res* 46:W315–W322. <https://doi.org/10.1093/nar/gky497>
- Nishi H, Hashimoto K, Panchenko Anna R (2011) Phosphorylation in protein-protein binding: effect on stability and function. *Structure* 19:1807–1815. <https://doi.org/10.1016/j.str.2011.09.021>
- Oeljeklaus S, Schummer A, Mastalski T, Platta HW, Warscheid B (2016) Regulation of peroxisome dynamics by phosphorylation. *BBA-Mol Cell Res* 1863:1027–1037. <https://doi.org/10.1016/j.bbamcr.2015.12.022>
- Okumoto K, El Shermely M, Natsui M, Kosako H, Natsuyama R, Marutani T, Fujiki Y (2020) The peroxisome counteracts oxidative stresses by suppressing catalase import via Pex14 phosphorylation. *Elife*. <https://doi.org/10.7554/eLife.55896>
- Olsen JV, de Godoy LMF, Li G, Macek B, Mortensen P, Pesch R, Makarov A, Lange O, Horning S, Mann M (2005) Parts per million mass accuracy on an orbitrap mass spectrometer via lock mass injection into a C-trap. *Mol Cell Proteomics* 4:2010–2021. <https://doi.org/10.1074/mcp.T500030-MCP200>
- Poirier Y, Antonenkov VD, Glumoff T, Hiltunen JK (2006) Peroxisomal β -oxidation—a metabolic pathway with multiple functions. *BBA-Mol Cell Res* 1763:1413–1426. <https://doi.org/10.1016/j.bbamcr.2006.08.034>
- Saleem RA, Rogers RS, Ratushny AV, Dilworth DJ, Shannon PT, Shteynberg D, Wan Y, Moritz RL, Nesvizhskii AI, Rachubinski RA, Aitchison JD (2010) Integrated phosphoproteomics analysis of a signaling network governing nutrient response and peroxisome induction. *Mol Cell Proteomics* 9:2076–2088. <https://doi.org/10.1074/mcp.M000116-MCP201>
- Schummer A, Maier R, Gabay-Maskit S, Hansen T, Mühlhäuser WWD, Suppanz I, Fadel A, Schuldiner M, Girzalsky W, Oeljeklaus S, Zalckvar E, Erdmann R, Warscheid B (2020) Pex14p Phosphorylation modulates import of citrate synthase 2 into peroxisomes in *saccharomyces cerevisiae*. *Front Cell Dev Biol* 8:955. <https://doi.org/10.3389/fcell.2020.549451>
- Sievers F, Wilm A, Dineen D, Gibson TJ, Karplus K, Li W, Lopez R, McWilliam H, Remmert M, Söding J, Thompson JD, Higgins DG (2011) Fast, scalable generation of high-quality protein multiple

- sequence alignments using clustal omega. *Mol Syst Biol* 7:539. <https://doi.org/10.1038/msb.2011.75>
- Smaczynska-de Rooij Iwona I, Marklew Christopher J, Allwood Ellen G, Palmer Sarah E, Booth Wesley I, Mishra R, Goldberg Martin W, Ayscough Kathryn R (2016) Phosphorylation regulates the endocytic function of the yeast dynamin-related protein Vps1. *Mol Cell Biol* 36:742–755. <https://doi.org/10.1128/MCB.00833-15>
- Subramani S, Koller A, Snyder WB (2000) Import of peroxisomal matrix and membrane proteins. *Annu Rev Biochem* 69:399–418. <https://doi.org/10.1146/annurev.biochem.69.1.399>
- Sula A, Cole AR, Yeats C, Orengo C, Keep NH (2014) Crystal structures of the human dysferlin inner DYSF domain. *BMC Struct Biol* 14:3–3. <https://doi.org/10.1186/1472-6807-14-3>
- Swaney DL, Beltrao P, Starita L, Guo A, Rush J, Fields S, Krogan NJ, Villén J (2013) Global analysis of phosphorylation and ubiquitylation cross-talk in protein degradation. *Nat Methods* 10:676–682. <https://doi.org/10.1038/nmeth.2519>
- Taylor SS, Keshwani MM, Steichen JM, Kornev AP (2012) Evolution of the eukaryotic protein kinases as dynamic molecular switches. *Philos Trans R Soc Lond Ser B Biol Sci* 367:2517–2528. <https://doi.org/10.1098/rstb.2012.0054>
- Thomas AS, Krikken AM, van der Klei IJ, Williams CP (2015) Phosphorylation of Pex11p does not regulate peroxisomal fission in the yeast *Hansenula polymorpha*. *Sci Rep* 5:11493. <https://doi.org/10.1038/srep11493>
- Vizeacoumar FJ, Torres-Guzman JC, Bouard D, Aitchison JD, Rachubinski RA (2004) Pex30p, Pex31p, and Pex32p form a family of peroxisomal integral membrane proteins regulating peroxisome size and number in *Saccharomyces cerevisiae*. *Mol Biol Cell* 15:665–677. <https://doi.org/10.1091/mbc.e03-09-0681>
- Vlastaridis P, Kyriakidou P, Chaliotis A, Van de Peer Y, Oliver SG, Amoutzias GD (2017) Estimating the total number of phosphoproteins and phosphorylation sites in eukaryotic proteomes. *GigaScience* 6:1–11. <https://doi.org/10.1093/gigascience/giw015>
- Wang W, Malcolm BA (1999) Two-stage PCR protocol allowing introduction of multiple mutations, deletions and insertions using quickchange site-directed mutagenesis. *Biotechniques* 26:680–682. <https://doi.org/10.2144/99264st03>
- Wang S, Idrissi F-Z, Hermansson M, Grippa A, Ejsing CS, Carvalho P (2018) Seipin and the membrane-shaping protein Pex30 cooperate in organelle budding from the endoplasmic reticulum. *Nat Commun* 9:2939. <https://doi.org/10.1038/s41467-018-05278-2>
- Zhang J, Tripathi DN, Jing J, Alexander A, Kim J, Powell RT, Dere R, Tait-Mulder J, Lee JH, Paull TT, Pandita RK, Charaka VK, Pandita TK, Kastan MB, Walker CL (2015) ATM functions at the peroxisome to induce pexophagy in response to ROS. *Nat Cell Biol* 17:1259–1269. <https://doi.org/10.1038/ncb3230>
- Zutphen T, Veenhuis M, van der Klei IJ (2008) Pex14 is the sole component of the peroxisomal translocon that is required for pexophagy. *Autophagy* 4:63–66. <https://doi.org/10.4161/auto.5076>

Publisher's Note Springer Nature remains neutral with regard to jurisdictional claims in published maps and institutional affiliations.